Inorganic Chemistry

Article

pubs.acs.org/IC

Novel Red-Emitting $Ba_2Tb(BO_3)_2Cl$:Eu Phosphor with Efficient Energy Transfer for Potential Application in White Light-Emitting Diodes

Zhiguo Xia,* Jiaqing Zhuang, and Libing Liao

School of Materials Science and Technology, China University of Geosciences, Beijing 100083, China

Supporting Information

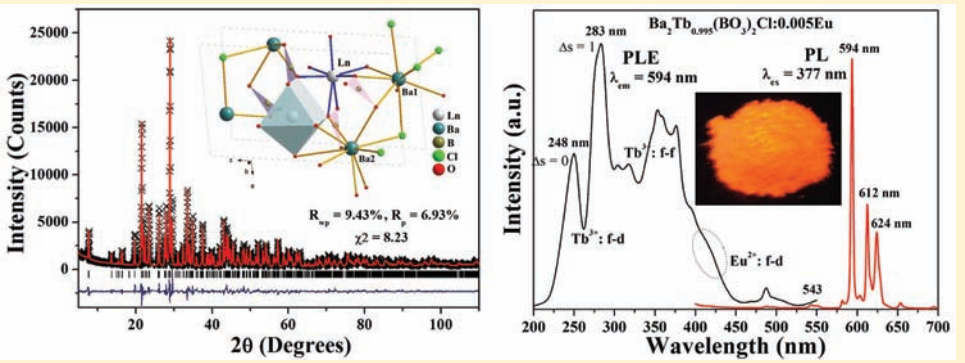

ABSTRACT: A novel red-emitting $Ba_2Tb(BO_3)_2Cl$:Eu phosphor possessing a broad excitation band in the near-ultraviolet (*n*-UV) region was synthesized by the solid-state reaction. Versatile $Ba_2Tb(BO_3)_2Cl$ compound has a rigid open framework, which can offer two types of sites for various valence's cations to occupy, and the coexistence of Eu^{2+}/Eu^{3+} and the red-emitting luminescence from Eu^{3+} with the aid of efficient energy transfer of Eu^{2+}−Eu^{3+}(Tb^{3+}) and Tb^{3+}−Eu^{3+} have been investigated. $Ba_2Tb(BO_3)_2Cl$ emits green emission with the main peak around 543 nm, which originates from $^5D_4 \rightarrow {}^7F_5$ transition of Tb^{3+}. $Ba_2Tb(BO_3)_2Cl$:Eu shows bright red emission from Eu^{3+} with peaks around 594, 612, and 624 nm under *n*-UV excitation (350−420 nm). The existence of Eu^{2+} can be testified by the broad-band excitation spectrum, UV−vis reflectance spectrum, X-ray photoelectron spectrum, and Eu L_3-edge X-ray absorption spectrum. Decay time and time-resolved luminescence measurements indicated that the interesting luminescence behavior should be ascribed to efficient energy transfer of Eu^{2+}−Eu^{3+}(Tb^{3+}) and Tb^{3+}−Eu^{3+} in $Ba_2Tb(BO_3)_2Cl$:Eu phosphors.

1. INTRODUCTION

Solid-state lighting based on InGaN semiconductors has attracted great attention due to the long lifetimes, high energy efficiency, compact structure, and environmental friendliness of white LEDs (*w*-LEDs).[1] Commercial *w*-LEDs generally employ a blue LED chip and a yellow light-emitting phosphor, which are very poor in the color rendering index (CRI) because of the color deficiency in the red region.[2] An alternative approach involves the manufacture of near-ultraviolet (*n*-UV) LED chips by blending red-, green-, and blue-emitting phosphors to assemble *w*-LEDs.[3] In particular, the external quantum efficiency of InGaN LEDs reaches a maximum at 400 nm, so that it is essential to develop novel phosphors that can be excited efficiently under *n*-UV irradiation, particularly red-emitting phosphors.[4] Phosphors containing Eu^{3+} ions as activators can emit red light, and their excitation bands usually consist of host lattice excitation bands, charge-transfer bands, and direct excitation bands of Eu^{3+} ions.[5] However, the host lattice excitation bands and charge-transfer bands usually locate at the short-wavelength UV region (<350 nm); moreover, direct excitation bands have some low and sharp absorption lines owing to the forbidden transition of Eu^{3+}.[5,6] As a comparison, the 4f−5d transition of the Eu^{2+} ion is sensitive to the crystal field and covalency, Eu^{2+}-doped phosphor generally shows superior absorption in the spectral region of 250−450 nm, which is equivalent to the emission of UV and *n*-UV LED chip, and they also exhibit broad emission bands from blue to red.[7] Therefore, as the characteristic broad-band transition excitation and emission of Eu^{2+} have been well recognized, it will be very exciting and interesting if an efficient Eu^{2+}−Eu^{3+} energy transfer happens in a single-phase valence-varied Eu-doped phosphor, which will offer us an opportunity to adjust the absorption of red-emitting phosphors containing Eu^{3+} ions.

Presently, abnormal mixed valences of Eu ions in some inorganic compounds have been studied by their controlling structural chemistry modification.[8−10] Orchestrating the coexistence of Eu^{2+}/Eu^{3+} activators in a single host lattice is still a daunting task, especially for the appearance of characteristic emission in order to generate white light.[8−12] However, we can utilize the absorption of Eu^{2+} and subsequent Eu^{2+}−Eu^{3+} energy transfer to obtain red-emitting luminescence upon *n*-UV excitation. Recently, we proposed a series of $Ba_2Ln(BO_3)_2Cl$ compounds (Ln = rare earth (RE) ions) and

Received: February 22, 2012
Published: June 11, 2012

studied the structure and luminescence properties of Eu^{2+}-doped $Ba_2Ln(BO_3)_2Cl$ (Ln = Y, Gd, and Lu) phosphors under *n*-UV light.[13−15] Therefore, we also synthesized a special phosphor host, $Ba_2Tb(BO_3)_2Cl$, in this $Ba_2Ln(BO_3)_2Cl$ (Ln = RE ions) series of compounds by introduction of Eu as the doping ions in order to explore the coexistence of Eu^{2+}/Eu^{3+} activators in a single host lattice. Furthermore, it is expected that the luminescence characteristic of the absorption of Eu^{2+} and subsequent Eu^{2+}−Eu^{3+} energy transfer can be used to obtain the red-emitting luminescence. It is found that, in comparison with the characteristic broad-band excitation and emission of Eu^{2+} in $Ba_2Ln(BO_3)_2Cl$ (Ln = Y, Gd, and Lu) phosphors, $Ba_2Tb(BO_3)_2Cl$:Eu phosphors show unusual luminescence behavior under *n*-UV excitation. $Ba_2Tb(BO_3)_2Cl$:Eu exhibits bright red emission from Eu^{3+} with a peak around 594, 612, and 624 nm owing to simultaneous absorption of Eu^{2+}, Eu^{3+}, and Tb^{3+} and their energy transfer. The existence of Eu^{2+} and the energy transfer between Eu^{2+} and Eu^{3+}(Tb^{3+}), Tb^{3+}, and Eu^{3+} in $Ba_2Tb(BO_3)_2Cl$:Eu phosphors have been discussed in detail.

2. EXPERIMENTAL SECTION

2.1. Sample Preparation. $Ba_2Tb(BO_3)_2Cl$ and $Ba_2Tb(BO_3)_2Cl$:Eu phosphors were prepared by the conventional high-temperature solid-state reaction in reductive atmosphere. The starting materials, $BaCO_3$ (99.95%), $BaCl_2{\cdot}2H_2O$ (99.95%), and H_3BO_3 (99.95%), were supplied by Sinopharm Chemical Reagent Co. Ltd., Shanghai, China, and Tb_4O_7 (99.995%) and Eu_2O_3 (99.995%) were supplied by China Minls (Beijing) Research Institute, Beijing, China. In a typical process, first, all starting materials were weighed according to the stoichiometric ratio and a 5% excess of H_3BO_3 was added to the mixture as flux. Then, these mixtures were ground evenly in an agate mortar and continually fired at 1000 °C for 3 h in the reductive atmosphere (5% H_2 + 95% N_2 mixed flowing gas). For comparison, $Ba_2Tb_{0.995}(BO_3)_2Cl$:0.005Eu phosphor was also prepared in air.

2.2. Sample Characterization. X-ray diffraction (XRD) patterns were recorded using an X-ray powder diffractometer (XRD-6000, SHIMADZU, Japan), operating at 40 kV, 30 mA. The continuous scanning rate (2θ ranging from 10° to 70°) used as phase formation determination was 4°(2θ)/min, and the step scanning rate (2θ ranging from 3° to 115°) used as Rietveld analysis was 8 s/step with a step size of 0.02. Powder diffraction data were obtained using the computer software General Structure Analysis System (GSAS) package.[16] Refined structure parameters comprised overall scale factors, lattice parameters, and fractional coordinates. Diffuse reflection spectra of samples were measured on a UV−visible−near-IR spectrophotometer (UV-3600, Shimadzu, Japan) attached to an integral sphere using $BaSO_4$ as a standard measurement. Photoluminescence (PL) and excitation (PLE) spectra were inspected using a fluorescent spectrophotometer (F-4600, HITACHI, Japan) with a photomultiplier tube operating at 400 V, and a 150 W Xe lamp was used as the excitation lamp. The room-temperature decay curves and time-resolved PL spectra were recorded on a JOBIN YVON FL3-21 spectrofluorometer, and 370 nm pulse laser radiation (nano-LED) was used as the excitation source. The internal quantum efficiency (η_{QE}) was measured using the integrating sphere (150 mm in diameter) on the FLS920 fluorescence spectrophotometer (Edinburgh Instruments Ltd., U.K.), and a Xe900 lamp was used as an excitation source and white $BaSO_4$ powder as a reference for correction of absorption. The signals were collected by a Hamamatsu R928P photomultiplier tube. X-ray photoelectron spectra (XPS) were measured in a PHI 5300 ESCA system, and an Al Kα X-ray source with a power of 250W was used. The pass energy of the analyzer was set at 55.00 eV, and the base pressure of the analysis chamber was better than 3×10^{-9} Torr. The charge effect was calibrated using the binding energy of C 1s (284.8 eV). The Eu L_3-edge X-ray absorption near-edge structure spectra (XAS) and vacuum ultraviolet (VUV) spectra were carried out by BL-17C and BL-03A, respectively, in the National Synchrotron Radiation Research Center (NSRRC) in Taiwan.

3. RESULTS AND DISCUSSIONS

3.1. Structure Analysis of $Ba_2Tb(BO_3)_2Cl$. Figure 1 and Table 1 give the Rietveld analysis patterns for X-ray powder diffraction data of $Ba_2Tb(BO_3)_2Cl$ host compound and its structural refinement results, respectively. $Ba_2Tb(BO_3)_2Cl$ compound is shown as the monoclinic space group of $P2_1/m$, which is the same as the previously reported $Ba_2Yb(BO_3)_2Cl$ compound.[17,18] Furthermore, the refined residual factors and unit cell parameters are summarized in Table 1. Compared with our recent work,[13−15] the unit cell parameters obtained for $Ba_2Tb(BO_3)_2Cl$ are a = 6.44978 Å, b = 5.32443 Å, c = 11.32274 Å, and β = 95.8549°, which are smaller than those for $Ba_2Gd(BO_3)_2Cl$ and larger than those for $Ba_2Ln(BO_3)_2Cl$ (Ln = Lu, Y, Yb), which were attributed to the Vegard rule and variation of these atomic radius. As pointed out in our recent work,[13] successful isomorphic substitution for Ln^{3+} sites in

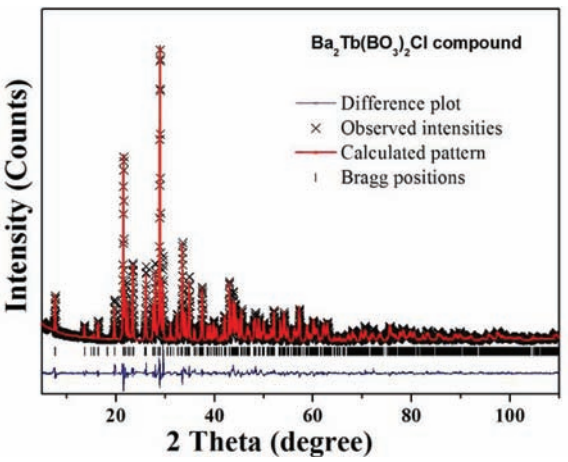

Figure 1. Rietveld analysis patterns for X-ray powder diffraction data of $Ba_2Tb(BO_3)_2Cl$ compound. Solid red lines are calculated intensities, and crosses are the observed intensities. Short vertical lines show the position of Bragg reflections of the calculated pattern. Blue solid lines below the profiles stand for the difference between the observed and the calculated intensities.

Table 1. Results of Structure Refinement of $Ba_2Tb(BO_3)_2Cl$

atoms	x	y	z	U_{iso}
Tb	0.3449	0.25	0.4112	0.02015
Ba1	0.3425	0.25	0.0743	0.02270
Ba2	0.0907	0.25	0.7082	0.02654
B1	0.3847	0.75	0.2034	0.05715
B2	0.7822	0.25	0.433	0.03859
Cl1	0.8503	0.25	0.0865	0.03676
O1	0.5093	0.75	0.1325	0.01695
O2	0.3069	0.5445	0.2643	0.01242
O3	0.9738	0.25	0.3996	0.02500
O4	0.6774	0.463	0.4413	0.02896
space group	reliability factors		cell params	
$P2_1/m$ (No. 11), monoclinic	χ^2 = 8.23 R_{wp} = 9.43% R_p = 6.93%		a = 6.4498(1) Å, b = 5.3244(1) Å, c = 11.3227(2) Å, β = 95.855(2)°, V = 386.81(1) Å^3, Z = 2	

dx.doi.org/10.1021/ic300401z | Inorg. Chem. 2012, 51, 7202−7209

$Ba_2Ln(BO_3)_2Cl$ by some trivalent rare earth ions, such as Sm, Eu, Gd, Tb, Dy, Ho, Er, Tm, Yb, Lu, and Y, has been verified. Figure S1, Supporting Information, further gives XRD patterns of as-prepared $Ba_2Tb(BO_3)_2Cl$ and $Ba_2Tb_{0.97}(BO_3)_2Cl$:0.03Eu phosphors. XRD results demonstrated that both of them crystallized in the same crystal phase of monoclinic $Ba_2Ln(BO_3)_2Cl$ structure, and introduction of dopants does not make any significant changes to the host.

In order to further understand the crystal structure and substitution of RE ions in $Ba_2Tb(BO_3)_2Cl$ host, Figure 2 presents the crystal structure of $Ba_2Tb(BO_3)_2Cl$ emphasizing the TbO_7 polyhedra and the coordination environment of cations (Tb1, Ba1, and Ba2). The versatile $Ba_2Tb(BO_3)_2Cl$ structure with its rigid open framework offers two types of sites for various cations to occupy, type I with trivalent Tb sites in TbO_7 polyhedra and type II with two different divalent Ba sites having 9-fold and 10-fold coordination. In this structure, the existing different types of sites are proved to be available for the guest cations with different charges to occupy. It is also found that the B atoms are triangular coordinated forming BO_3 groups, and they share edges or corners with Ba polyhedra to form a three-dimensional network, as shown in Figure 2. For an open borate framework, they also supply the possibility for different doping RE ions, such as the coexistence of Eu^{2+} and Eu^{3+}. In the present work, the ionic radii of Ba^{2+}, Tb^{3+}, Eu^{2+}, and Eu^{3+} are 1.52, 1.12, 1.25, and 1.15 Å. Therefore, it could offer the possible opportunity for Eu^{2+}−Ba^{2+} and Eu^{3+}−Tb^{3+} substitution owing to the structure constraints when the $Ba_2Tb(BO_3)_2Cl$:Eu sample was prepared in a reductive atmosphere. However, the valence stability of RE ions in a specific host is a very complicated phenomenon, and some work on the explanation of the intrinsic mechanism is still in progress.[8,19]

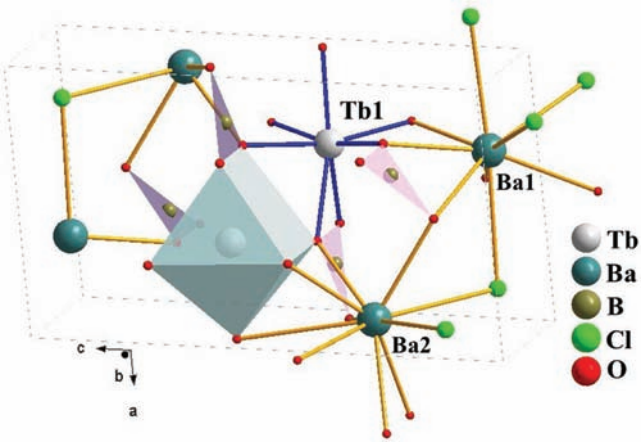

Figure 2. Crystal structure of $Ba_2Tb(BO_3)_2Cl$ emphasizing the TbO_7 polyhedra and the coordination environment of cations (Tb1, Ba1, and Ba2).

3.2. Photoluminescence Properties of $Ba_2Tb(BO_3)_2Cl$:Eu Phosphor. The possibility of the Eu^{2+}/Eu^{3+} coexistence deduced from crystal chemistry analysis can be verified by the photoluminescence property.[11,12,20] Figure 3 shows the PLE and PL spectra of $Ba_2Tb(BO_3)_2Cl$ and $Ba_2Tb_{0.995}(BO_3)_2Cl$:0.005Eu phosphors. As given in Figure 3, the PL spectrum of $Ba_2Tb(BO_3)_2Cl$ under 377 nm *n*-UV excitation consists of several narrow characteristic f−f transition emission lines of Tb^{3+} with a main peak centered at 543 nm,

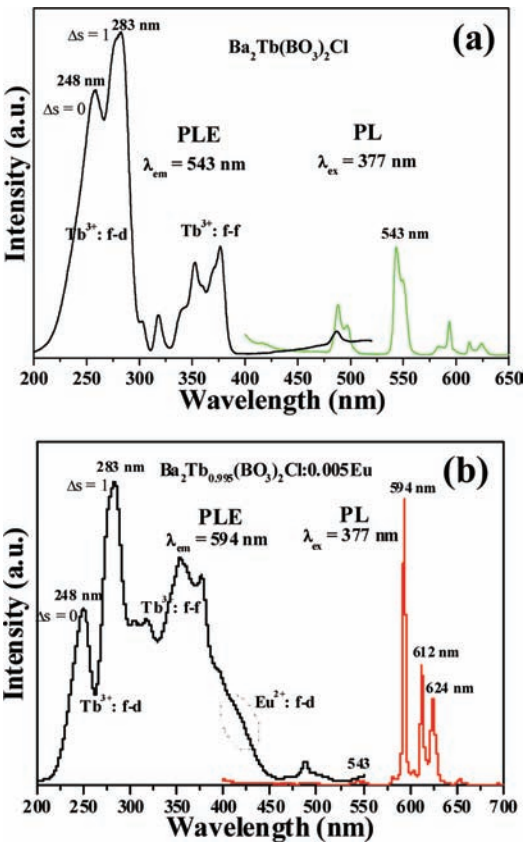

Figure 3. PLE and PL spectra of $Ba_2Tb(BO_3)_2Cl$ (a) and $Ba_2Tb_{0.995}(BO_3)_2Cl$:0.005Eu (b) phosphor.

which originates from the $^5D_4 \rightarrow {}^7F_5$ transition of Tb^{3+}.[21] However, once the Eu ions with a very low concentration of 0.005 mol were introduced into this matrix in the reductive atmosphere, Tb^{3+} emission suffered obvious luminescence quenching and there was a remarkable enhancement on the emission intensities at 594, 612, and 624 nm for $Ba_2Tb_{0.995}(BO_3)_2Cl$:0.005Eu phosphor. It can be proposed that the narrow emission peaks around 594, 612, and 624 nm should be corresponding to the electric dipole transitions of $^5D_0 \rightarrow {}^7F_1$, $^5D_0 \rightarrow {}^7F_2$, and $^5D_0 \rightarrow {}^7F_2$ transition of Eu^{3+}.[22] This result demonstrates that the $Ba_2Tb(BO_3)_2Cl$:Eu phosphor is a promising red-emitting component that may be applied to *w*-LEDs excited using *n*-UV LED chips. A more exciting thing is that the excitation band of $Ba_2Tb(BO_3)_2Cl$:Eu phosphor has been widened obviously owing to introduction of Eu dopant in this interesting $Ba_2Tb(BO_3)_2Cl$ host. As shown in Figure 3a, the excitation spectrum of $Ba_2Tb(BO_3)_2Cl$ exhibits two obvious broad bands from 200 to 300 nm with two peaks at 248 and 283 nm and some weak transitions from 300 to 400 nm. The two broad structured plateau with maxima at 248 and 283 nm should correspond to a spin-allowed $4f^8-4f^75d^1$ ($^7F_6-{}^7D$) transition with higher energy (248 nm, $\Delta S = 0$) and a spin-forbidden $4f^8-4f^75d^1$ ($^7F_6-{}^9D$) transition with lower energy (283 nm, $\Delta S = 1$) of Tb^{3+} ion, respectively.[22,23] The other sharp lines in the long-wavelength regions can be assigned to the f−f transition of Tb^{3+} ions. The above similar phenomenon has also been found in the $TbBO_3$ host.[22] Similarly, $Ba_2Tb(BO_3)_2Cl$:Eu phosphor possesses the same excitation band in the short-wavelength region coming from the Tb-containing host, as shown in Figure 3b. However, the intensity of the sharp lines corresponding to the transition of Tb^{3+} has

dx.doi.org/10.1021/ic300401z | *Inorg. Chem.* 2012, 51, 7202−7209

been enhanced obviously, and the excitation band edge has been broadened to 450 nm, showing a broad-band character. Figure S2 in the Supporting Information gives the emission spectrum of $Ba_2Tb_{0.995}(BO_3)_2Cl$:0.005Eu phosphor achieved by 420 nm excitation, which exhibit similarities by comparing the relative intensities of the emission lines from Eu^{3+} 4f–4f transitions. Thus, it proves the bright red-emitting luminescence under *n*-UV excitation (350–420 nm).

In general, we can propose that the enhancement of the red-emitting luminescence can be ascribed to the energy transfer from Tb^{3+} to Eu^{3+}.[20] Part of the increase of the excitation peaks of $Ba_2Tb_{0.995}(BO_3)_2Cl$:0.005Eu phosphor in the *n*-UV region should result from the appearance of the charge transfer band of Eu–O and the transition of Eu^{3+} ions after introduction of Eu into the $Ba_2Tb(BO_3)_2Cl$ host. However, it cannot completely explain the broad excitation band and notable broadening at the *n*-UV absorption edge. As proposed previously, $Ba_2Tb(BO_3)_2Cl$:Eu prepared in a reductive atmosphere would offer the chance for Eu^{2+}–Ba^{2+} and Eu^{3+}–Tb^{3+} substitution simultaneously. Moreover, we observed broad-band excitation and emission of Eu^{2+} ions in the isomorphic $Ba_2Ln(BO_3)_2Cl$ (Ln = Y, Gd, Lu) host.[13−15] Although red-emitting luminescence of Eu^{3+} dominates in the $Ba_2Tb_{0.995}(BO_3)_2Cl$:0.005Eu phosphor, it cannot prevent formation of Eu^{2+} in this versatile $Ba_2Ln(BO_3)_2Cl$ compound. Owing to the strong red-emitting lines of Eu^{3+}, Eu^{2+} emission in $Ba_2Tb(BO_3)_2Cl$ cannot exhibit the obvious characteristic broad-band emission as previously reported in $Ba_2Gd(BO_3)_2Cl$:Eu^{2+} phosphor.[13] However, minor Eu^{2+} ions play an important role in the broadening excitation band, which helps form the f–d transition excitation of Eu^{2+}. In order to verify this speculation, Figure 4 shows the excitation spectra

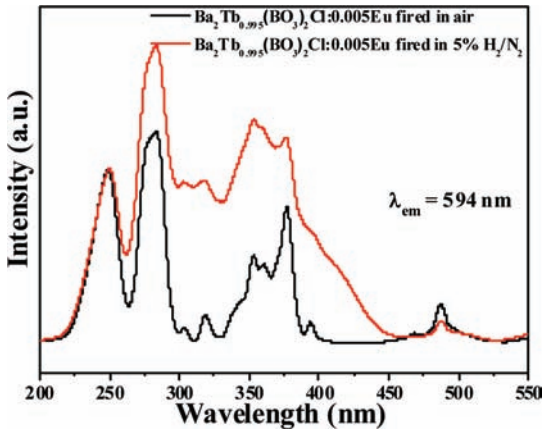

Figure 4. Excitation spectra (λ_{em} = 594 nm) of $Ba_2Tb_{0.995}(BO_3)_2Cl$:0.005Eu phosphors obtained at different experimental conditions.

(λ_{em} = 594 nm) of $Ba_2Tb_{0.995}(BO_3)_2Cl$:0.005Eu phosphors obtained at different experimental conditions. $Ba_2Tb_{0.995}(BO_3)_2Cl$:0.005Eu phosphor is prepared in air, and there is an obvious difference in the excitation band owing to the appearance of the broad excitation band, which supports the existence of Eu^{2+} mentioned above. Furthermore, Figure S3, Supporting Information, shows the emission spectra (λ_{ex} = 377 nm) of $Ba_2Tb_{0.995}(BO_3)_2Cl$:0.005Eu phosphors prepared under different atmosphere. It is found that the emission intensity of $Ba_2Tb_{0.995}(BO_3)_2Cl$:0.005Eu phosphor fired in air is relatively lower than that of the $Ba_2Tb_{0.995}(BO_3)_2Cl$:0.005Eu phosphors prepared in 5% H_2/N_2, suggesting the possibility of Eu^{2+} absorption and efficient energy transfer between Eu^{2+}–Eu^{3+}(Tb^{3+}).

Figure 5 shows the reflectance spectra of $Ba_2Tb(BO_3)_2Cl$ and $Ba_2Tb_{0.995}(BO_3)_2Cl$:0.005Eu phosphor. The $Ba_2Tb(BO_3)_2Cl$ host shows a strong energy absorption band in the 250–340 nm region, which agrees well with the f–d transition of Tb^{3+}, as found in the excitation spectrum. Except for this, the narrow absorption lines at 377 and 486 nm should be ascribed to the f–f transition of Tb^{3+}. As a comparison, $Ba_2Tb_{0.995}(BO_3)_2Cl$:0.005Eu phosphor shows an obvious broad absorption band near 400 nm, which should be caused by the $4f^7$–$4f^65d^1$ transition of Eu^{2+}.[24] The reflectance spectrum and PLE spectrum results show that the absorption of $Ba_2Tb(BO_3)_2Cl$:Eu phosphor matches well with the emission of *n*-UV chips; thus, $Ba_2Tb(BO_3)_2Cl$:Eu has the potential as a promising candidate for solid-state lighting. Furthermore, to better understand the effect of Eu concentration on the emission intensity of the phosphor, PL spectra of $Ba_2Tb_{1-z}(BO_3)_2Cl$:*z*Eu phosphors were systematically studied. Figure 6 gives the PL spectra of $Ba_2Tb_{1-z}(BO_3)_2Cl$:*z*Eu phosphors under 377 nm UV excitation. It can be seen that the emission intensities at 594 nm of these series of phosphors

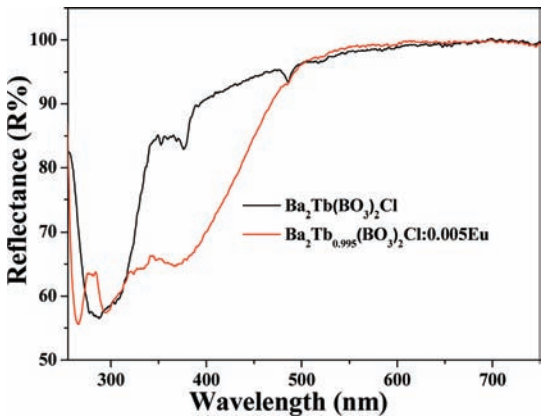

Figure 5. Reflectance spectra of $Ba_2Tb(BO_3)_2Cl$ and $Ba_2Tb_{0.995}(BO_3)_2Cl$:0.005Eu phosphor.

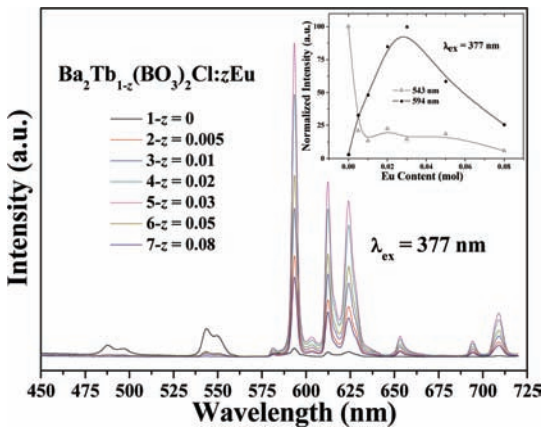

Figure 6. PL spectra of $Ba_2Tb_{1-z}(BO_3)_2Cl$:*z*Eu (*z* = 0, 0.005, 0.01, 0.02, 0.03, 0.05, 0.08) phosphors under *n*-UV excitation (λ_{ex} = 377 nm), and (inset) variation of the normalized intensities at 543 and 594 nm emission corresponding to the Eu content.

dx.doi.org/10.1021/ic300401z | Inorg. Chem. 2012, 51, 7202–7209

increased rapidly with increasing content of Eu from 0.005 to 0.03 mol and then declined dramatically with further increasing Eu content, as shown in the inset of Figure 6. The emission intensities at 543 nm decreased significantly with introduction of Eu dopant and was kept at a low value with little difference. It is believed that concentration quenching of the Eu^{3+} emission at 594 nm and efficient $Tb^{3+} \rightarrow Eu^{3+}$ energy transfer can be used to explain the above Eu doping concentration-dependent luminescence behavior.

3.3. Evidence of Eu^{2+}/Eu^{3+} Coexistence in $Ba_2Tb(BO_3)_2Cl$:Eu Phosphor. Although Eu^{2+}/Eu^{3+} coexistence has been reported in many materials,[8−12] some direct evidence should be given for the present $Ba_2Tb(BO_3)_2Cl$:Eu phosphor in order to explain the observed luminescence behavior. XPS technique is suitable to study the chemical states of europium.[25,26] The XPS survey spectrum of $Ba_2Tb_{0.97}(BO_3)_2Cl$:0.03Eu phosphor is shown in Figure S4, Supporting Information, which revealed photoelectron peaks corresponding to Ba 3d, Ba 4d, O KLL, Tb 4d, B 1s, Cl 1s, Cl 2s, Cl 2p, and Eu 3d emissions. The high-resolution XPS spectrum at the Eu 3d position is shown in Figure S5, Supporting Information. There are two peaks around 1124 and 1135 eV, and the shapes and binding energies of the Eu 3d signals in $Ba_2Tb_{0.995}(BO_3)_2Cl$:0.005Eu agree well with the signals of Eu^{2+} $3d_{5/2}$ and Eu^{3+} $3d_{5/2}$, respectively.[26] Although the peak around 1124 eV ascribed to Eu^{2+} $3d_{5/2}$ is very weak, the coexistence of Eu^{2+} and Eu^{3+} in the $Ba_2Tb_{0.97}(BO_3)_2Cl$:0.03Eu phosphors can be inferred from the present XPS spectrum. However, it is very hard to characterize the exact relative ratio of Eu^{2+}/Eu^{3+} in the $Ba_2Tb(BO_3)_2Cl$:Eu phosphor owing to the low doping concentration of the Eu ion. However, the relative Eu^{2+}/Eu^{3+} ratio should be fixed in the same experimental conditions in our work.

Accordingly, XPS can only be used to analyze the surface of phosphors. In order to further investigate the internal valence, the sample was tested with XAS at the photon energy around the Eu L_3 edge.[27] Figure 6 presents the Eu L_3-edge XAS spectra of $Ba_2Tb_{0.97}(BO_3)_2Cl$:0.03Eu, and the Eu L_3-edge XAS spectra of $Ba_2Gd_{0.97}(BO_3)_2Cl$:0.03Eu^{2+}, commercial $BaMgAl_{10}O_{17}$:Eu^{2+}, and Y_2O_3:Eu^{3+} were also used as a reference. As demonstrated by the XAS spectra of $Ba_2Gd_{0.97}(BO_3)_2Cl$:0.03Eu^{2+}, commercial $BaMgAl_{10}O_{17}$:Eu^{2+}, and Y_2O_3:Eu^{3+}, Eu^{2+} and Eu^{3+} show two peaks around 6975 and 6984 eV, which originate from the $^2p_{3/2} \rightarrow 5d$ electron transition in Eu^{2+} and Eu^{3+}, respectively. In Figure 7, the peak around 6984 eV can be clearly found and the peak around 6975 eV corresponding to Eu^{2+} is very weak, as marked by the dotted rectangle. It can be easily deduced that the weaker the peak around 6975 eV, the lower the concentration of Eu^{2+} can be formed in the sample. Therefore, this result is in agreement with our speculation on the existence of minor Eu^{2+} in $Ba_2Tb(BO_3)_2Cl$:Eu phosphor, which is also verified by the former XPS measurements. Formation of a minor amount of Eu^{2+} in $Ba_2Tb(BO_3)_2Cl$:Eu phosphor should be the competing effect of the open crystallographic sites (Tb^{3+} and Ba^{2+}) and the reductive atmosphere and ability. The possible process can be inferred as follows: (1) in the process of the phase formation period of $Ba_2Tb(BO_3)_2Cl$, Eu^{3+} will act as the chemical component in the Tb^{3+} sites to build the $Ba_2Tb(BO_3)_2Cl$ framework and the redox reaction will happen preferably for $Tb^{4+}-Tb^{3+}$ not $Eu^{3+}-Eu^{2+}$ in 5% H_2/95% N_2 atmosphere; (2) in the process of the valence-varied Eu formation period, the

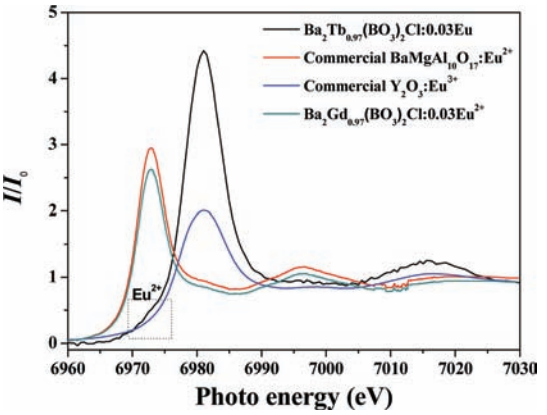

Figure 7. Eu L_3-edge XAS spectra of $Ba_2Tb_{0.97}(BO_3)_2Cl$:0.03Eu, and Eu L_3-edge XAS spectra of $Ba_2Gd_{0.97}(BO_3)_2Cl$:0.03Eu^{2+}, commercial $BaMgAl_{10}O_{17}$:Eu^{2+}, and Y_2O_3:Eu^{3+} used as the reference.

minor part of the Eu^{3+} in Tb^{3+} sites will be reduced to Eu^{2+}. However, the $Ba_2(Tb,Eu)(BO_3)_2Cl$ three-dimensional network is structurally stable, only a little Eu^{2+} can be obtained, even the redox reaction happens in 25% H_2/75% N_2 atmosphere and the reaction time is prolonged to 24 h in our experiment. Therefore, novel red-emitting $Ba_2Tb(BO_3)_2Cl$:Eu^{2+}/Eu^{3+} phosphor with a fixed Eu^{2+}/Eu^{3+} ratio can be obtained under the given experimental condition.

3.4. Energy Transfer and Luminescence Mechanism in $Ba_2Tb(BO_3)_2Cl$:Eu Phosphor. According to the discussion mentioned above, the quenching of Tb^{3+} around 543 nm should be ascribed to efficient energy transfer of $Tb^{3+}-Eu^{3+}$.[22,28] On the other hand, the obvious excitation band broadening in the *n*-UV region and the difference of PL/PLE spectra for $Ba_2Tb(BO_3)_2Cl$:Eu phosphor prepared in reductive and air atmosphere proved the contribution of Eu^{2+} and $Eu^{2+}-Eu^{3+}(Tb^{3+})$ energy transfer. In our recent report, we observed and verified the $Eu^{2+}-Tb^{3+}$ energy transfer in the $Ba_2Lu(BO_3)_2Cl$:Eu^{2+}/Eu^{3+},Tb^{3+} system.[15] In this work, we also find the efficient energy transfer of $Eu^{2+}-Tb^{3+}$ and $Eu^{2+}-Eu^{3+}$ and the subsequent $Tb^{3+}-Eu^{3+}$ energy transfer process. Therefore, Figure 8 displays the proposed diagram of energy transfer between $Tb^{3+}-Eu^{3+}$ and $Eu^{2+}-Eu^{3+}(Tb^{3+})$ in the $Ba_2Tb(BO_3)_2Cl$:Eu phosphors. As can be seen from Figure 8, the

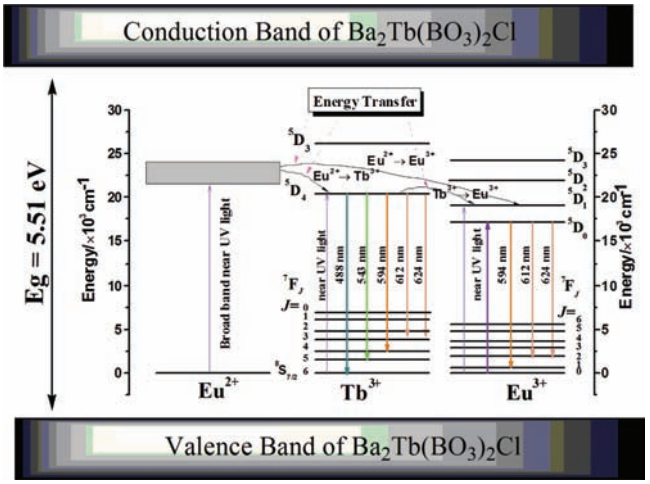

Figure 8. Schematic energy level diagram showing the energy transfer among Eu^{2+}, Tb^{3+}, and Eu^{3+} in $Ba_2Tb(BO_3)_2Cl$:Eu phosphor.

dx.doi.org/10.1021/ic300401z | Inorg. Chem. 2012, 51, 7202−7209

excitation lines of $Ba_2Tb(BO_3)_2Cl$:Eu phosphors in the *n*-UV region come from the absorption of the combined effect of Tb^{3+}, Eu^{3+}, and Eu^{2+}, so that a wide and strong absorption band can be observed in the PLE spectrum (Figure 3b). The absorbed energy of Tb^{3+} could be transferred from the $^5D_4$ level of Tb^{3+} to the $^5D_0$ ($^5D_1$) level of Eu^{3+}; accordingly, the absorbed energy of Eu^{2+} can also be completely transferred from the $4f^65d^1$ band to the $^5D_1$ level of Eu^{3+} and the $^5D_4$ level of Tb^{3+}. As also given in Figure S6, Supporting Information, it shows the VUV excitation and emission spectra of the $Ba_2Tb(BO_3)_2Cl$ host compound. The broad band centered at ca. 225 nm is assigned to be the host absorption band, viz., the transition from the valence band to the conduction band. According to the formula of $E = 1240/\lambda$, the energy difference of the valence band and conduction band is calculated to be 5.51 eV, as shown in the energy level diagram of Figure 8. Moreover, the VUV emission spectrum of $Ba_2Tb(BO_3)_2Cl$ (Figure S6, Supporting Information) consists of several individual sharp lines, and the peaks at 488, 543, 594, and 612/624 nm were assigned to the $^5D_4$–^7F_J (J = 6, 5, 4, and 3) transitions of Tb^{3+} ions, respectively, which is similar to the PL spectrum discussed above (Figure 3a).

To investigate the energy transfer process from Tb^{3+} to Eu^{3+}, their decay curves were recorded. The room-temperature decay curves and lifetimes of Eu^{3+} emission at 594 nm and Tb^{3+} emission at 543 nm of $Ba_2Tb(BO_3)_2Cl$ and $Ba_2Tb_{0.995}(BO_3)_2Cl$:0.005Eu phosphors are shown in Figure 9. As shown in Figure 9, the decay curves of the $^5D_4 \rightarrow {}^7F_5$ transition (Tb^{3+} emission at 543 nm) in $Ba_2Tb(BO_3)_2Cl$ and $^5D_0 \rightarrow {}^7F_1$ transition (Eu^{3+} emission at 594 nm) in $Ba_2Tb_{0.995}(BO_3)_2Cl$:0.005Eu phosphor are well fitted by a first-order exponential function

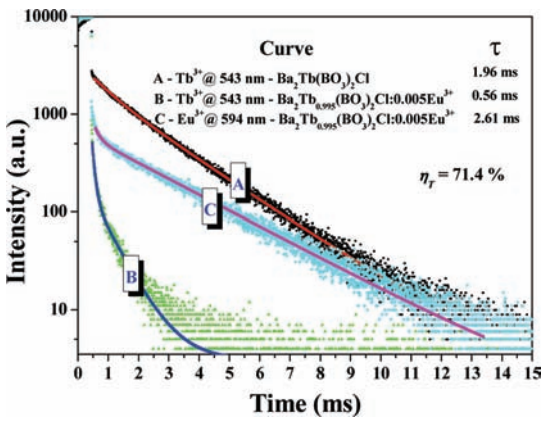

Figure 9. Decay time curves and lifetimes of Eu^{3+} in $Ba_2Tb_{0.995}(BO_3)_2Cl$:0.005Eu phosphor (C) and Tb^{3+} in $Ba_2Tb(BO_3)_2Cl$ (A) and $Ba_2Tb_{0.995}(BO_3)_2Cl$:0.005Eu phosphor (B).

$$I(t) = A \exp(-t/\tau) \quad (1)$$

where I is the luminescence intensity at time t, A is constant, t is the time, and τ is the decay time for the exponential components. On the basis of eq 1 and decay curves, the decay times were determined to be 1.96 and 2.61 ms for the $^5D_4 \rightarrow {}^7F_5$ and $^5D_0 \rightarrow {}^7F_1$ transitions, respectively, as also given in Figure 9. However, it is found that energy transfer results in the corresponding changes in the decay curves. The PL decay curve of the $^5D_4 \rightarrow {}^7F_5$ transition (Tb^{3+} emission at 543 nm) in $Ba_2Tb_{0.995}(BO_3)_2Cl$:0.005Eu phosphor can be well fitted with a biexponential equation as given in the following expression[5]

$$I = A_1 \exp(-t/\tau_1) + A_2 \exp(-t/\tau_2) \quad (2)$$

where I is the luminescence intensity at time t, t is the time, A_1 and A_2 are constants, and τ_1 and τ_2 are the decay times for the exponential components. Moreover, the average lifetime (τ^*) can be determined using the calculation below

$$\tau^* = (A_1\tau_1^2 + A_2\tau_1^2)/(A_1\tau_1 + A_2\tau_1) \quad (3)$$

Consequently, it can be seen from Figure 9 that the lifetime of Tb^{3+} at 543 nm was determined to be 0.56 ms once 0.5% mol Eu was introduced into the $Ba_2Tb(BO_3)_2Cl$ host. We also measured the decay time curves and lifetimes of the $^5D_4 \rightarrow {}^7F_5$ transition (Tb^{3+} emission at 543 nm) in $Ba_2Tb_{1-z}(BO_3)_2Cl$:zEu phosphor with different Eu content, as given in Figure S7, Supporting Information. It was found the decay times decreased with increasing Eu content, which also confirmed efficient energy transfer. Therefore, the result demonstrates that the energy transfer process occurs between sensitizer Tb^{3+} and acceptor Eu^{3+} in $Ba_2Tb(BO_3)_2Cl$:Eu phosphors. Accordingly, the energy transfer efficiency from Tb^{3+} to Eu^{3+} can be calculated according to the following expression[29]

$$\eta_T = 1 - \frac{\tau_x}{\tau_0} \quad (4)$$

where τ_0 is the lifetime of the sensitizer Tb^{3+} of the samples in the absence of acceptor Eu^{3+}, τ_x is the lifetime of Tb^{3+} in the presence of Eu^{3+}, and η_T is the energy transfer efficiency. As presented in Figure 9, the total energy transfer efficiency (η_T) was determined to be 71.4% from Tb^{3+} to Eu^{3+} in the $Ba_2Tb_{0.995}(BO_3)_2Cl$:0.005Eu phosphor.

As discussed previously, the intense emission Eu^{3+} results from efficient energy transfer from Tb^{3+} to Eu^{3+} in the $Ba_2Tb(BO_3)_2Cl$:Eu phosphors. In order to obtain more information about the kinetic properties of the energy transfer process from Tb^{3+} to Eu^{3+},[30] the room-temperature time-resolved emission spectra of Tb^{3+} and Eu^{3+} in $Ba_2Tb_{0.995}(BO_3)_2Cl$:0.005Eu phosphor were measured by exciting into the absorption of Tb^{3+} using a 370 nm laser with a delay time ranging from 0 to 5.0 ms (Figure 10). At t = 0, the typical emission of Tb^{3+} from $^5D_3$–^7F_J (J = 6, 5, 4, 3, 2) can be observed simultaneously, indicating that two processes occur in the excited Tb^{3+}: one is the radiative transitions to the ground state of Tb^{3+} and the other nonradiative transfer of the Eu^{3+} (as shown in the energy level diagram of Figure 8). As also shown in Figure 10, when t = 1.25 ms, the emission of Tb^{3+} at 543 nm decreased obviously due to the short lifetime of Tb^{3+} in $Ba_2Tb_{0.995}(BO_3)_2Cl$:0.005Eu phosphor (τ = 0.56 ms) and the emission peaks around 594, 612, and 624 nm corresponding to the $^5D_0 \rightarrow {}^7F_1$, $^5D_0 \rightarrow {}^7F_2$, and $^5D_0 \rightarrow {}^7F_2$ transitions of Eu^{3+} became dominant due to efficient energy transfer of Tb^{3+} to Eu^{3+}. Therefore, the Eu^{3+} ion acts as the terminal of the energy transfer processes in the $Ba_2Tb(BO_3)_2Cl$:Eu phosphor. Thus, we can obtain bright red luminescence in the $Ba_2Tb(BO_3)_2Cl$:Eu phosphor.

Figure 11 depicts the CIE chromaticity diagram for $Ba_2Tb_{1-z}(BO_3)_2Cl$:zEu phosphors with different Eu contents, and two photographs of the selected phosphors are also embedded in the diagram as a reference. In addition, the relative CIE chromaticity coordinates for the $Ba_2Tb_{1-z}(BO_3)_2Cl$:zEu phosphors are given in Table 2. It can

dx.doi.org/10.1021/ic300401z | Inorg. Chem. 2012, 51, 7202–7209

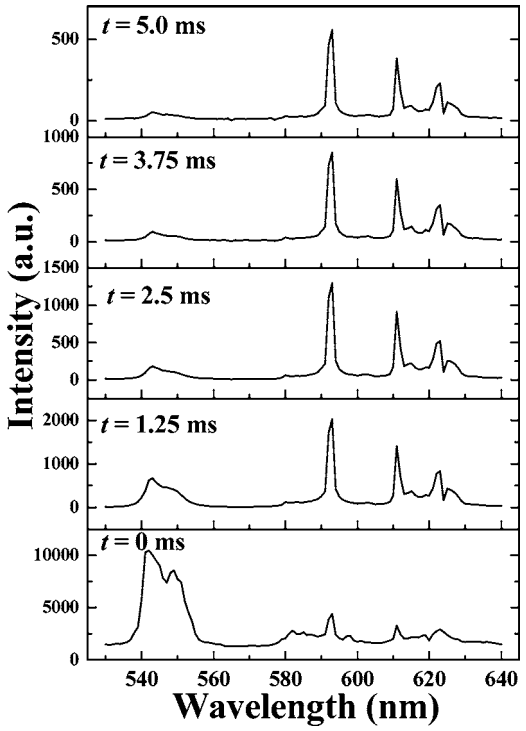

Figure 10. Time-resolved emission spectra of $Ba_2Tb_{0.995}(BO_3)_2Cl$:0.005Eu phosphor under 370 nm excitation.

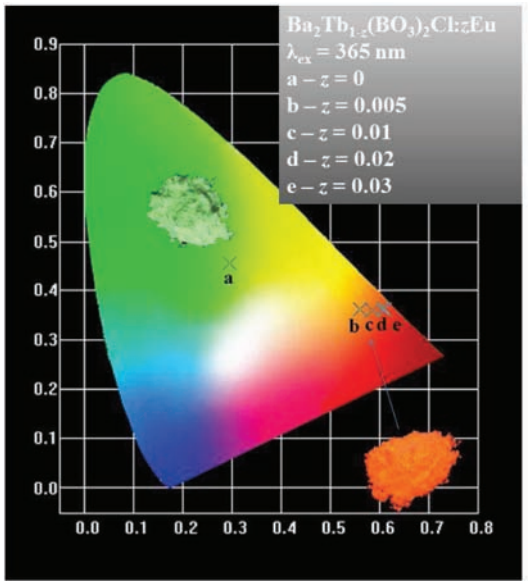

Figure 11. CIE chromaticity diagram and typical phosphor images (under 365 nm UV lamp) of $Ba_2Tb_{1-z}(BO_3)_2Cl$:zEu (z = 0, 0.005, 0.01, 0.02, 0.03).

be seen from Figure 11 that the color tone or hue of these phosphors can be tuned from the pale green (Figure 11a) to the red (Figure 11e) area, which corresponds to chromaticity coordinates (x, y) varying from (0.296, 0.454) to (0.611, 0.363). Considering the photographs in Figure 11a and 11c, it is clearly observed that the $Ba_2Tb_{1-z}(BO_3)_2Cl$:zEu phosphors show an intense red-emitting color due to the energy transfer of Tb^{3+}–Eu^{3+} and Eu^{2+}–Eu^{3+}(Tb^{3+}). The internal quantum efficiency (QE) of $Ba_2Tb_{0.97}(BO_3)_2Cl$:0.03Eu phosphor, measured under 377 nm excitation at room temperature, is

Table 2. CIE Chromaticity Coordinates for $Ba_2Tb_{1-z}(BO_3)_2Cl$:zEu under 377 nm Excitation

	$Ba_2Tb_{1-z}(BO_3)_2Cl$:zEu samples	chromaticity coordinates	
no.	z	x	y
a	0	0.296	0.454
b	0.005	0.561	0.362
c	0.01	0.584	0.359
d	0.02	0.604	0.364
e	0.03	0.611	0.363

56% (detailed calculations are provided in the Supporting Information, Figure S8), which is a little lower than that of the reported commercial red-emitting phosphor $Sr_2Si_5N_8$:Eu^{2+} (79%).[31] However, the QE can be improved by controlling the particle size, size distribution, morphology, and crystalline defects through optimization of the processing conditions and composition.

4. CONCLUSIONS

The new red-emitting phosphors of $Ba_2Tb(BO_3)_2Cl$:Eu were synthesized using the conventional solid-state reaction. The excitation spectrum of $Ba_2Tb(BO_3)_2Cl$:Eu in the range of 200–500 nm monitoring the red emission peak at 594 nm reveals several bands corresponding to the $4f^8$–$4f^75d$ transition of Tb^{3+}, charge transfer transition of Tb^{3+}–O^{2-}, f–f transition of Tb^{3+} and Eu^{3+} ions, and broad-band absorption of the f–d transition of Eu^{2+} ions, respectively. The coexistence of Eu^{2+}/Eu^{3+} can be proved by indirect PL and UV–vis reflectance spectra measurement and direct evidence of the XPS and Eu L_3-edge XAS results. Accordingly, the combined processes of the energy transfer occur from Eu^{2+} to Eu^{3+}(Tb^{3+}) and Tb^{3+} to Eu^{3+} at the same time in the $Ba_2Tb(BO_3)_2Cl$:Eu phosphor. The energy transfer efficiency of Tb^{3+}–Eu^{3+} was roughly calculated as 71.4%, and the kinetic properties of the energy transfer process from Tb^{3+} to Eu^{3+} were verified by the time-resolved emission spectra. Bright red-emitting luminescence from Eu^{3+} with peaks around 594, 612, and 624 nm under n-UV excitation (350–420 nm) can be realized in this novel phosphor system by the combined energy transfer processes. The measured internal quantum efficiency of $Ba_2Tb_{0.97}(BO_3)_2Cl$:0.03Eu phosphor is 56%. This new finding in $Ba_2Tb(BO_3)_2Cl$:Eu phosphor on the broad-band absorption in n-UV region and realization of red-emitting luminescence ascribed to the energy transfer will provide a new way to explore the novel red-emitting phosphor used in white LEDs.

■ ASSOCIATED CONTENT

Ⓢ Supporting Information

XRD patterns of $Ba_2Tb(BO_3)_2Cl$ and $Ba_2Tb_{0.97}(BO_3)_2$-Cl:0.03Eu phosphor; emission spectra of $Ba_2Tb_{0.995}(BO_3)_2$-Cl:0.005Eu phosphor for different excitation wavelengths of λ_{ex} = 377 nm and 420 nm; emission spectra (λ_{ex} = 377 nm) of $Ba_2Tb_{0.995}(BO_3)_2Cl$:0.005Eu phosphors obtained at different experimental conditions; XPS survey spectrum and high-resolution XPS spectrum at the Eu3d position of $Ba_2Tb_{0.97}(BO_3)_2Cl$:0.03Eu phosphor prepared in 5% H_2/N_2; VUV excitation and emission spectra of $Ba_2Tb(BO_3)_2Cl$ host compound; decay time curves and lifetimes of Tb^{3+} (543 nm) in $Ba_2Tb_{1-z}(BO_3)_2Cl$:zEu phosphor; detailed calculations and reference figure on the quantum efficiency. This material is available free of charge via the Internet at http://pubs.acs.org.

dx.doi.org/10.1021/ic300401z | Inorg. Chem. 2012, 51, 7202–7209

AUTHOR INFORMATION

Corresponding Author

*Phone: +86-10-8233-2247. Fax: +86-10-8232-2974. E-mail: xiazg426@yahoo.com.cn.

Notes

The authors declare no competing financial interest.

ACKNOWLEDGMENTS

This research was supported by the National Natural Science Foundations of China (Grant No.51002146), the Ph.D. Programs Foundation of the Ministry of Education of China (Grant No. 20090022120002), the Fundamental Research Funds for the Central Universities (2010ZY35, 2011YYL005), and the Funds of the State Key Laboratory of Rare Earth Resource Utilization, Changchun Institute of Applied Chemistry, Chinese Academy of Sciences (RERU2011014). The authors thank Prof. Ru-Shi Liu in National Taiwan University and NSRRC in Taiwan for providing the VUV and XAS measurements.

REFERENCES

(1) (a) Nakamura, S.; Fasol, G. *Proc. SPIE−Int. Soc. Opt. Eng.* **1997**, *3002*, 26. (b) Bachmann, V.; Ronda, C.; Meijerink, A. *Chem. Mater.* **2009**, *21*, 2077. (c) Setlur, A. A.; Radkov, E. V.; Henderson, C. S.; Her, J.-H.; Srivastava, A. M.; Karkada, N.; Kishore, M. S.; Kumar, N. P.'; Aesram, D.; Deshpande, A.; Kolodin, B.; Grigorov, L. S.; Happek, U. *Chem. Mater.* **2010**, *22*, 4076.

(2) (a) Blasse, G.; Bril, A. *J. Chem. Phys.* **1967**, *47*, 5139. (b) Setlur, A. A.; Heward, W. J.; Gao, Y.; Srivastava, A. M.; Chandran, R. G.; Shankar, M. V. *Chem. Mater.* **2006**, *18*, 3314. (c) Hoppe, H. A. *Angew. Chem., Int. Ed.* **2009**, *48*, 3572.

(3) (a) Saradhi, M. P.; Varadaraju, U. V. *Chem. Mater.* **2006**, *18*, 5267. (b) Huang, C. H.; Chen, T. M. *Inorg. Chem.* **2011**, *50*, 5725. (c) Liu, W. R.; Huang, C. H.; Wu, C. P.; Chiu, Y. C.; Yeh, Y. T.; Chen, T. M. *J. Mater. Chem.* **2011**, *21*, 6869.

(4) (a) Kang, D. S.; Yoo, H. S.; Jung, S. H.; Kim, H. K.; Jeon, D. Y. *J. Phys. Chem. C* **2011**, *115*, 24334. (b) Du, F. P.; Zhu, R.; Huang, Y. L.; Tao, Y.; Seo, H. J. *Dalton Trans.* **2011**, *40*, 11433.

(5) Blasse, G.; Grabmaier, B. C. *Luminescent Materials*; Springer-Verlag: Berlin, 1994.

(6) Wang, Z.; Liang, H.; Wang, Q.; Luo, L.; Gong, M. *Mater. Sci. Eng., B* **2009**, *164*, 120. (b) Ye, S.; Xiao, F.; Pan, Y. X.; Ma, Y. Y.; Zhang, Q. Y. *Mater. Sci. Eng. R* **2010**, *71*, 1. (c) Xia, Z. G.; Sun, J. F.; Du, H. Y; Chen, D. M.; Sun, J. Y. *J. Mater. Sci.* **2010**, *45*, 1553.

(7) (a) Xia, Z. G.; Sun, J. Y.; Du, H. Y.; Zhou, W. *Opt. Mater.* **2006**, *28*, 524. (b) Chiu, Y. C.; Huang, C. H.; Lee, T. J.; Liu, W. R.; Yeh, Y. T.; Jang, S. M.; Liu, R. S. *Opt. Express* **2011**, *19*, A331. (c) Xia, Z. G.; Du, H. Y.; Sun, J. Y.; Chen, D. M.; Wang, X. F. *Mater. Chem. Phys.* **2010**, *119*, 7.

(8) (a) Dorenbos, P. *Chem. Mater.* **2005**, *17*, 6452. (b) Zeuner, M.; Pagano, S.; Matthes, P.; Bichler, D.; Johrendt, D.; Harmening, T.; Pottgen, R.; Schnick, W. *J. Am. Chem. Soc.* **2009**, *131*, 11242.

(9) Saradhi, M. P.; Pralong, V.; Varadaraju, U. V.; Raveau, B. *Chem. Mater.* **2009**, *21*, 1793.

(10) Pawar, A. U.; Jadhav, A. P.; Pal, U.; Kim, B. K.; Kang, Y. S. *J. Lumin.* **2012**, *132*, 659.

(11) Mao, Z. Y.; Wang, D. J.; Lu, Q. F.; Yu, W. H.; Yuan, Z. H. *Chem. Commun.* **2009**, 346.

(12) Mao, Z. Y.; Wang, D. J. *Inorg. Chem.* **2010**, *49*, 4922.

(13) Xia, Z. G.; Wang, X. M.; Wang, Y. X.; Liao, L. B.; Jing, X. P. *Inorg. Chem.* **2011**, *50*, 10134.

(14) Xia, Z. G.; Zhuang, J. Q.; Liao, L. B.; Liu, H. K.; Luo, Y.; Du, P. *J. Electrochem. Soc.* **2011**, *158*, J359.

(15) Xia, Z. G.; Zhuang, J. Q.; Liu, H. K.; Liao, L. B. *J. Phys. D: Appl. Phys.* **2012**, *45*, 015302.

(16) (a) Larson, A. C.; Von Dreele, R. B. General Structure Analysis System (GSAS); *Los Alamos National Laboratory Report LAUR 86-748*; Los Alamos National Laboratory: Los Alamos, NM, 1994. (b) Toby, B. H. *J. Appl. Crystallogr.* **2001**, *34*, 210.

(17) Khamaganova, T. N.; Nevskii, N. N.; Trunov, V. K. *Sov. Phys. Cryst.* **1989**, *34*, 853.

(18) Schipper, W. J.; Blasse, G. *J. Alloys Compd.* **1994**, *203*, 267.

(19) Song, Z.; Liao, J.; Ding, X. L.; Zhou, T. L.; Liu, Q. L. *J. Lumin.* **2012**, *132*, 1768.

(20) Le, F. H.; Wang, L. X.; Jia, W.; Jia, D. Z.; Bao, S. J. *J. Alloys Compd.* **2012**, *512*, 323.

(21) (a) Li, G. G.; Geng, D. L.; Shang, M. M.; Zhang, Y.; Peng, C.; Cheng, Z. Y.; Lin, J. *J. Phys. Chem. C* **2011**, *115*, 21882. (b) Chuang, H. Y.; Lu, C. H.; Hsu, C. H. *J. Am. Ceram. Soc.* **2010**, *93*, 1838.

(22) Yang, J; Zhang, C. M.; Li, C. X.; Lin, J. *Inorg. Chem.* **2008**, *47*, 7262.

(23) (a) Hsu, C. H.; Lu, C. H. *J. Mater. Chem.* **2011**, *21*, 2932. (b) Park, W. B.; Singh, S. P.; Pyo, M.; Sohn, K. S. *J. Mater. Chem.* **2011**, *21*, 5780.

(24) (a) Xia, Z. G.; Du, P.; Liao, L. B.; Li, G. W.; Jin, S. *Curr. Appl. Phys.* **2010**, *10*, 1087. (b) Krings, M.; Montana, G.; Dronskowski, R.; Wichleder, C. *Chem. Mater.* **2011**, *23*, 1694.

(25) Vercaemst, R.; Poelman, D.; Fiermans, L.; Van Meirhaeghe, R. L.; Laflere, W. H.; Cardon, F. *J. Electron Spectrosc. Relat. Phenom.* **1995**, *74*, 45.

(26) Chae, K. W.; Park, T. R.; Cheon, C. I.; Cho, N. I; Kim, J. S. *J. Lumin.* **2011**, *131*, 2597.

(27) Yang, L. X.; Xu, X.; Hao, L. Y.; Wang, Y. F.; Yin, L. J.; Yang, X. F.; He, W.; Li, Q. X. *J. Phys. D: Appl. Phys.* **2011**, *44*, 355403.

(28) (a) Hao, Z. D.; Zhang, J. H.; Zhang, X.; Lu, S. Z.; Wang, X. J. *J. Electrochem. Soc.* **2009**, *156*, H193. (b) Bettinelli, M.; Piccinelli, F.; Speghini, A.; Ueda, J.; Tanabe, S. *J. Lumin.* **2012**, *132*, 27.

(29) (a) Yang, W. J.; Chen, T. M. *Appl. Phys. Lett.* **2006**, *88*, 101903. (b) Yu, J. Y.; Hao, Z. D.; Zhang, X.; Luo, Y. S.; Zhang, J. H. *Chem. Commun.* **2011**, *47*, 12376.

(30) (a) Yu, M.; Wang, H.; Lin, C. K.; Li, G. Z.; Lin, J. *Nanotechnology* **2006**, *17*, 3245. (b) Hou, Z. Y.; Wang, L. L.; Lian, H. Z.; Chai, R. T.; Zhang, C. M.; Cheng, Z. Y.; Lin, J. *J. Solid State Chem.* **2009**, *182*, 698.

(31) Xie, R. J.; Hirosaki, N.; Kimura, N.; Sakuma, K.; Mitomo, M. *Appl. Phys. Lett.* **2007**, *90*, 191101.